Available online at www.sciencedirect.com
ScienceDirect
Journal of Solid State Chemistry 180 (2007) 2933–2941
JOURNAL OF SOLID STATE CHEMISTRY
www.elsevier.com/locate/jssc

Photon cascade luminescence in $CaAl_{12}O_{19}$:Pr, Cr

Z.G. Nie[a,b], J.H. Zhang[a,b,*], X. Zhang[a,b], S.Z. Lü[a,b], X.G. Ren[a,b], G.B. Zhang[c], X.J. Wang[a,b,d,*]

[a]*Key Laboratory of Excited State Physics, Changchun Institute of Optics, Fine Mechanics and Physics, Chinese Academy of Sciences, 16 Eastern Nan-Hu Road, Changchun 130033, China*
[b]*Graduate School of Chinese Academy of Sciences, Beijing 100039, China*
[c]*National Synchrotron Radiation Laboratory, University of Science and Technology of China, Hefei 230029, China*
[d]*Department of Physics, Georgia Southern University, Statesboro, GA 30460, USA*

Received 2 July 2007; received in revised form 18 August 2007; accepted 21 August 2007
Available online 6 September 2007

Abstract

In this report, the Cr^{3+} ion was chosen as a co-dopant to modify the unpractical photon cascade emission properties of Pr^{3+}-doped $CaAl_{12}O_{19}$ phosphors, which emit one near-UV photon from the $^1S_0$ state followed by visible photons from the $^3P_0$ state, into phosphors that emits two visible photons through energy transfer. The photon cascade emission process via energy transfer and the transfer mechanisms were systemically investigated by luminescence spectra and dynamics using synchrotron radiation as one of the excitation sources. The internal visible quantum efficiency of $CaAl_{12}O_{19}$:Pr, Cr was estimated and compared with $CaAl_{12}O_{19}$:Pr and the drawback to obtain the visible quantum efficiency higher than unit for $CaAl_{12}O_{19}$:Pr, Cr as a practical VUV phosphor was also discussed.

Keywords: Photon cascade luminescence; Synchrotron radiation; Energy transfer

1. Introduction

The development of plasma display panels and mercury-free fluorescent lamps in recent years made new demands for the efficient VUV-excited phosphors [1]. In these applications, the high energy of the VUV photons produced by the rare gas discharge make it possible to achieve two visible photon emissions for one VUV photon absorbed, namely a phosphor quantum efficiency (QE) higher than unit [2]. The successive emission of two photons, so-called photon cascade emission (PCE), was observed in Pr^{3+}-doped materials when the energy level of $^1S_0$ ($4f^2$) is located below the lowest $4f5d$ energy level [3–5]. Incident VUV photons are absorbed by Pr^{3+} from its ground state ($^3H_4$) into the $4f5d$ configuration. After relaxation, the excitation decays to the $^1S_0$ state. Then $^1S_0$ is depopulated through a two-step cascade emission, involving transitions $^1S_0$–$^1I_6$ (around 402 nm) followed by $^3P_0$–^3F_J, ^3H_J (480–700 nm). Thus a system with internal QE greater than unit can be achieved. But this two-photon luminescence is not monochromatic and the first step transition, $^1S_0$–$^1I_6$, is near the UV range, not suitable for practical application. Therefore, an appropriate co-dopant that can modify the unpractical PCE properties by converting the first step photon into proper visible photon through energy transfer (ET) could be a solution for this situation [6–11].

Oxide materials are usually better choices than fluoride materials for VUV phosphor because of its relatively easier preparation method and higher VUV absorption efficiency although most of the Pr^{3+}-based PCE hosts are fluorides [3,12]. Pr^{3+}-based PCE in oxides was discovered several years ago in Pr^{3+}-doped $SrAl_{12}O_{19}$ [13], $LaMgB_5O_{10}$ [14], and LaB_3O_6 [15], etc. In this present work, $CaAl_{12}O_{19}$ (CAO) was selected as a host to incorporate Pr^{3+} and Cr^{3+} to investigate the possibility of using Cr^{3+} co-doping to modify the PCE properties of Pr^{3+}. CAO is also a host in

*Corresponding authors. Key Laboratory of Excited State Physics, Changchun Institute of Optics, Fine Mechanics and Physics, Chinese Academy of Sciences, 16 Eastern Nan-Hu Road, Changchun 130033, China. Fax: +86 431 86176317.
E-mail addresses: zhangjh@ciomp.ac.cn (J.H. Zhang), xwang@georgiasouthern.edu (X.J. Wang).

0022-4596/$ - see front matter © 2007 Elsevier Inc. All rights reserved.
doi:10.1016/j.jssc.2007.08.024

which the lowest $4f5d$ level of Pr^{3+} is located above its $^1S_0$ ($4f^2$) level. The trivalent chromium, Cr^{3+}, is a promising candidate for this kind of co-dopant because Cr^{3+} has abundant energy levels in the range from UV to visible, and Cr^{3+} itself has efficient red emission in CAO host.

2. Experimental section

2.1. Sample preparation

Microcrystalline CAO:Pr, CAO:Cr and CAO:Pr, Cr phosphors were synthesized by high-temperature solid-state reaction method using $CaCO_3$ (99.99%), γ-Al_2O_3 (99.999%), Pr_6O_{11} (99.99%), MgO (99.999%) and Cr_2O_3 (99.99%) (all from Beijing Fine Chemical Company) as raw materials. The choice of this type of Al_2O_3 powder as a starting material is based on its high reactivity [16]. Powders of the raw materials were dried at 200 °C for 12 h in air to remove any water. Stoichiometric amounts of the starting materials above were weighed and then wet-mixed in 2-propyl alcohol (>97%) for 5 h in an agate container with agate balls on a planetary mill. After mixing, the 2-propyl alcohol was evaporated. The powder was dried in a stove for 1 day at 200 °C, and a small amount of H_3BO_3 as a flux was added and then it was subsequently ground for 1 h in an agate mortar. The powder was fired in a molybdenum crucible under CO reducing atmosphere, which was formed by activated carbon at high temperature. Reactions were performed in a vertical high-temperature tube furnace at 1550 °C for 10 h, and then quenched to room temperature. The final processes of grinding and firing were repeated two times. The heating rates of 5 °C/min were used.

The Pr^{3+} concentration of 1% (in mol) along with Cr^{3+} concentrations of 1%, 2%, 3%, 4%, 5%, 6%, 7% and 10% and the Cr^{3+} concentration of 1% along with Pr^{3+} concentrations of 1%, 3% and 5% were used in the preparation process. When Pr^{3+} is doped, equivalent amounts of Mg^{2+} were co-doped, substituting for Al^{3+} for charge compensation [17].

2.2. Characterizations

All the measurements were performed at room temperature. The powder diffraction data were obtained by X-ray diffraction (XRD) using a Cu target radiation resource ($\lambda = 1.54078$ Å). The VUV excitation spectra in the region of 130–330 nm were measured at the VUV station of the BS-U10B beam-line in National Synchrotron Radiation Laboratory, Hefei, China. The typical spectral resolutions of the primary monochromator (1 m Seya-Namioka) and the secondary monochromator (Spectrapro-275) are 0.4 and 2 nm, respectively. The pressure in the vacuum chamber during the measurements was 1×10^{-4} Pa. The excitation and emission spectra were detected by a Hamamatsu H5920-01 photomultiplier. The excitation spectra were corrected for the photoflux of the excitation beam using the excitation spectrum of sodium salicylate as standard. Fluorescence and excitation spectra in the UV region were obtained by Hitachi F-4500 Fluorescence Spectrophotometer, which equipped with a continuous 150-W Xe-arc lamp. For comparison of different samples, the spectra were measured with the same instrument parameters (2.5 nm for the excitation slit, 2.5 nm for the emission slit and 700 V for the PMT voltage). The emission spectra have been corrected for the response of the detector. The fluorescence dynamics of Pr^{3+} and Cr^{3+} were detected with a Tektronix digital oscilloscope model TDS 3052. An optical parametric oscillator was used as the excitation source. It has a line width of 0.2 cm^{-1}, pulse duration of 10 ns and repetition frequency of 10 Hz.

3. Results and discussion

3.1. Crystal structure

CAO adopts a hexagonal magnetoplumbite structure, crystallizing in space group $P6_3/mmc$ [18]. The XRD patterns of the host CAO (a) as well as CAO:Pr (b) and CAO:Cr (c) samples, both with high dopant concentration, are shown in Fig. 1. The d-spacing (d, crystal plane spacing) of some peaks is presented. First, they are all in good agreement with JCPDS No. 84-1613, and no additional phase is observed. Second, relative to the host

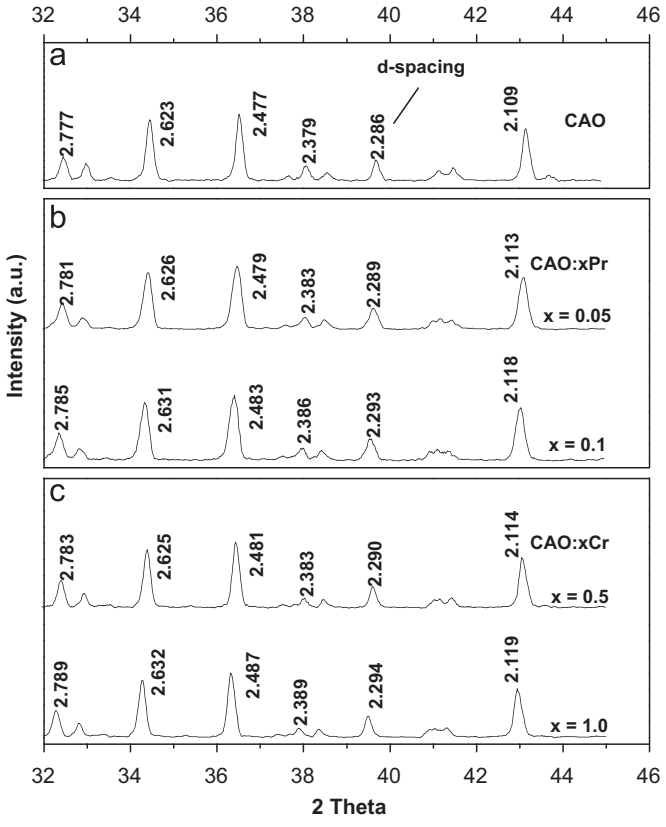

Fig. 1. XRD patterns of CAO (a), CAO:Pr (b) and CAO:Cr (c). The d-spacing of some peaks is given in this figure.

CAO, the d of each peak increases with increasing Pr^{3+} and Cr^{3+} concentrations. According to Bragg's Law, $n\lambda = 2d\sin\theta$, the increase of d results from the fact that the ion size of doped ions is larger than the replaced ions in a crystal. For CAO:Pr, the ion sizes of Pr^{3+} (~126.6 pm; all radii taken from Ref. [19]) and Ca^{2+} ions (~126 pm) are about equal. Thus, the increase of d may result from the co-doped big Mg^{2+} ions (71 pm, 4-coord.) substituting for the small Al^{3+} (53 pm, 4-coord.) in the spinel block, as they do in $SrAl_{12}O_{19}$. For CAO:Cr, the ion size of Cr^{3+} ions (75.5 pm, 6-coord.) is larger than that of Al^{3+} (67.5 pm, 6-coord.) and much smaller than that of Ca^{2+} ions (~126 pm). Then the increase of d is attributed to the fact that Cr^{3+} substitutes for Al^{3+} site in the host.

The ET efficiency of the Forster–Dexter type depends on the spectral overlap between Pr^{3+} emission and co-activator absorption as well as on their separation [20,21]. Both strongly depend on the type of host lattice. Wang et al. [17] reported the observation of ET between Pr^{3+} and Er^{3+} in CAO. However, both rare-earth ions replace Ca^{2+} sites in the host. Although the dopant concentrations are relatively high, the large molecule that contains only one Ca makes big separation between the donor and acceptor, leading to a small ET rate. In the CAO unit cell, the Ca^{2+} ion is surrounded by Al^{3+} ions and the distance of Ca–Ca (~10.95 Å, evaluated from the date in Ref. [18]) is much larger than the average separation of Ca–Al (~4.64 Å). In this work, Cr^{3+} replaces Al^{3+} in the host. The average D–A distance for Cr^{3+} co-doping is shorter than that for RE^{3+} co-doping for the same doping concentration. According to Dexter's theory, the ET efficiency depends on the average D–A separation in the host [21]. The shorter D–A distance may benefit the ET between Pr^{3+} and Cr^{3+}.

3.2. Spectral overlap and possibility of PCE in CAO:Pr, Cr

The VUV excitation and emission spectrum of CAO:1% Pr is shown in Fig. 2(a). The bands in the VUV excitation spectrum are the absorptions of Pr^{3+} 4*f*5*d* states. Upon 205 nm excitation of the 4*f*5*d* states, the emission lines of Pr^{3+} at 214, 254, 275, 341, 402 and 485 nm are assigned to $^1S_0$–$^3H_4$, $^3F_4$, $^1G_4$, $^1D_2$, $^1I_6$ and $^3P_0$–$^3H_4$ transitions, respectively, and the emissions of $^1S_0$–$^1I_6$ and $^3P_0$–$^3H_4$ constitute the two-step PCE process [13–15]. The UV and VUV excitation and emission spectra of CAO:1% Cr are shown in Fig. 2(b). The broad band dominated at 184 nm is ascribed to the O^{2-}–Cr^{3+} related charge transfer band (CTB) [22]. In the UV excitation spectrum, the three bands at 575, 419 and 264 nm belong to the spin-allowed transitions from the $^4A_2$ to the $^4T_2$, $^4T_1$(F) and $^4T_1$(P) states of Cr^{3+}, respectively [23]. The emission of CAO:Cr consists of a ^2E–$^4A_2$ zero-phonon line peaking at 686 nm with some vibronic sidebands [23]. The comparison of the emission spectrum of CAO:Pr and the excitation spectrum of CAO:Cr reveals that the two-step Pr^{3+} cascade emissions $^1S_0$–$^1I_6$ at 402 nm and $^3P_0$–$^3H_4$ at 485 nm overlap

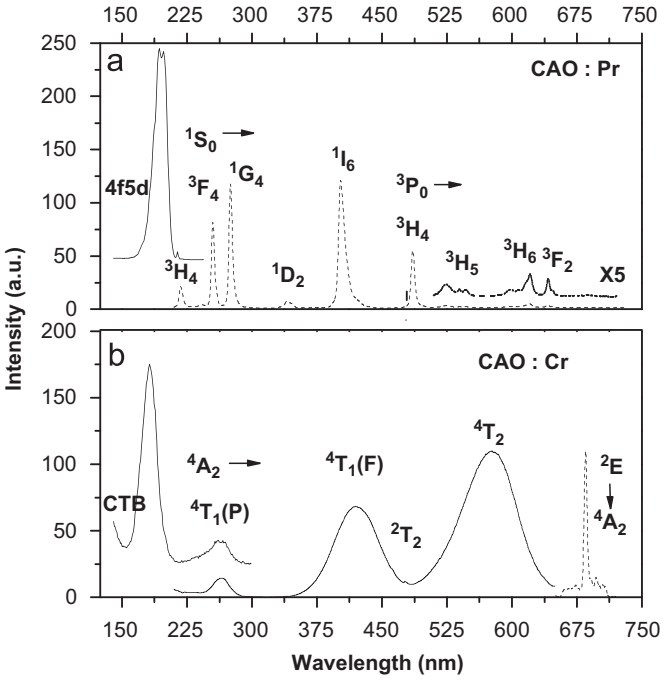

Fig. 2. (a) VUV excitation spectrum (solid line) of CAO:Pr monitoring the Pr^{3+} emission at 402 nm and the emission spectrum (dashed line) upon 4*f*5*d* excitation at 205 nm. (b) UV and VUV excitation spectra (solid lines) of the Cr^{3+} 686 nm emission (dashed line) in CAO:Cr. The UV and VUV excitation spectra are scaled to the $^4A_2$–$^4T_1$(P) excitation intensity.

Cr^{3+} excitations $^4A_2$–$^4T_1$(F) and $^4A_2$–$^4T_2$ states, respectively. According to Dexter's theory [21], in Pr^{3+}–Cr^{3+} co-doped CAO system, PCE could be achieved by ETs from Pr^{3+} $^1S_0$ and $^3P_0$ states to Cr^{3+} under these resonant conditions, i.e., the successive emissions of Pr^{3+} $^1S_0$ and $^3P_0$ states are both possible to be converted into the luminescence of Cr^{3+}, and then the unpractical PCE properties of Pr^{3+} can be modified.

Part of the energy-level scheme for the Pr^{3+}–Cr^{3+} system in CAO, showing the possibility of using Cr^{3+} co-doping to modify the PCE properties of Pr^{3+} via a two-step ET, is presented in Fig. 3. Firstly, upon excitation to the lowest 4*f*5*d* states of Pr^{3+}, part of the excitation energy is transferred to Cr^{3+} by cross-relaxation, exciting Cr^{3+} to the $^4T_1$(F) state and bringing Pr^{3+} to the $^1I_6$ level (denoted by CR_i). Secondly, after the electrons quickly relax from $^1I_6$ down to ^3P_J [24], the remaining excitation also can be transferred to a high-energy state of Cr^{3+} (denoted by ET_p). Each step can result in a red emission due to the Cr^{3+} ^2E–$^4A_2$ transition. It should be noted that CR_i can depopulate the Pr^{3+} $^1S_0$ state, feed the high-energy states of Cr^{3+} and simultaneously populate the $^1I_6$ level of Pr^{3+}. Consequently, an *increase* of the relative emission intensity of $^3P_0$ to $^1S_0$ is expected in CAO:Pr, Cr compared to that in CAO:Pr if CR_i occurs. The occurrence of CR_i can therefore be evaluated by comparing the emission spectra upon Pr^{3+} 4*f*5*d* states excitation in samples with and without Cr^{3+} co-doping.

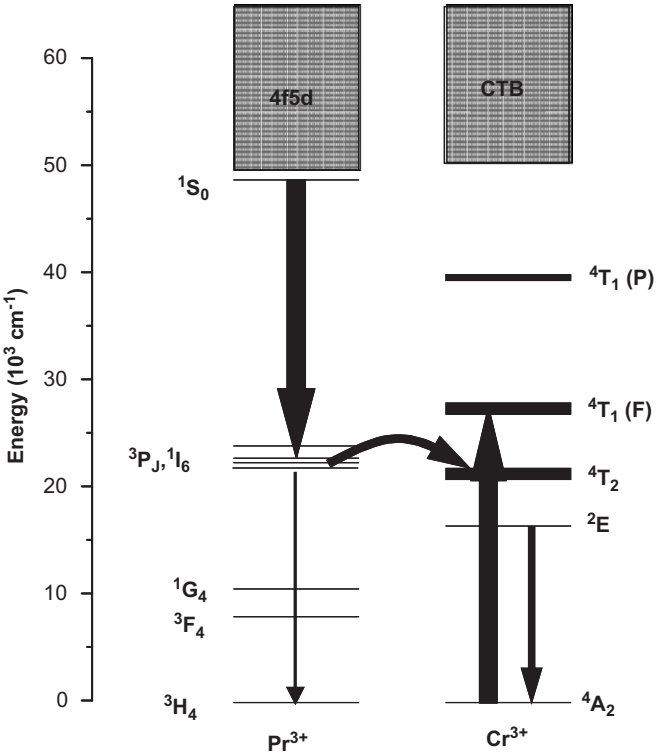

Fig. 3. Energy level diagram of the Pr^{3+}–Cr^{3+} system in CAO, showing the possibility of using Cr^{3+} co-doping to modify the PCE properties of Pr^{3+} via ET.

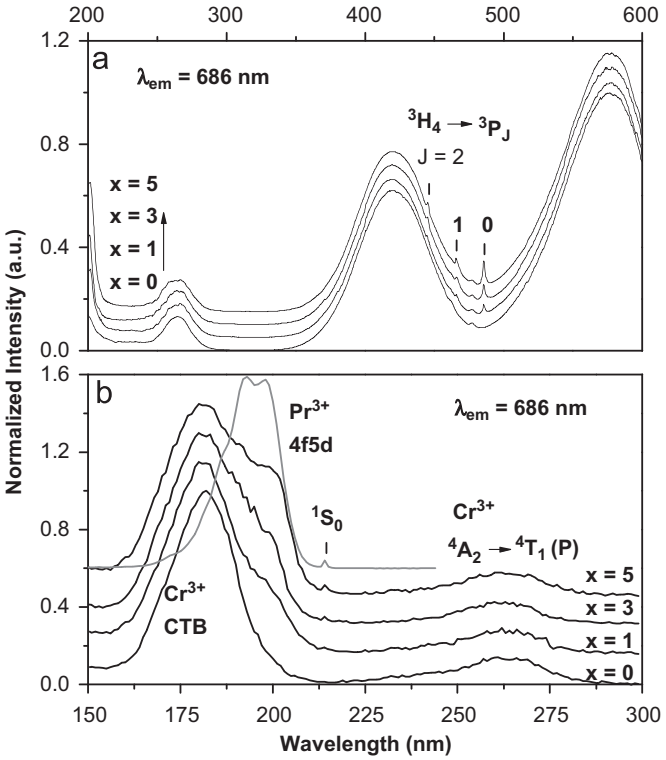

Fig. 4. Normalized UV (a) and VUV (b) excitation spectra of the Cr^{3+} 686 nm emission in CAO:1% Cr, x% Pr ($x = 0$, 1, 3, 5). The spectra have been offset vertically for clarity.

In addition, there are also spectral overlaps between $^1S_0$–$^3F_4$, $^1G_4$ Pr^{3+} emissions and the $^4A_2$–$^4T_1$(P) Cr^{3+} absorption, as shown in Fig. 2. Thus the emission energies of Pr^{3+} $^1S_0$–$^3F_4$, $^1G_4$ also could be transferred to Cr^{3+} through cross-relaxations (denoted by CR_f and CR_g, respectively). However, after the electrons relax from $^1S_0$ down to $^3F_4$ or $^1G_4$ through cross-relaxations, the remaining energy could not be transferred to Cr^{3+} and also no visible emissions could be yielded. But the contribution to this transfer is equivalent to the direct ET of all excitation energy from Pr^{3+} $^1S_0$ state to a high Cr^{3+} state (denoted by ET_S), and also could result in a red photon on Cr^{3+}.

3.3. Spectroscopic investigation of PCE via ET in CAO:Pr, Cr

Fig. 4 presents the UV (a) and VUV (b) excitation spectra of the Cr^{3+} emission at 686 nm in CAO:1% Cr, x% Pr ($x = 0$, 1, 3, 5). The peaks of Pr^{3+} $^3H_4$–$^3P_0$ (485 nm), $^3P_1$ (465 nm), $^3P_2$ (445 nm), belong to spin forbidden transitions, appear in the UV excitation spectra of Cr^{3+} emission and grow up with increasing x, indicating the occurrence of ET from Pr^{3+} ^3P_J to Cr^{3+}. In the VUV excitation spectra, the additional contributions locating on the right shoulder of the O^{2-}–Cr^{3+}-related CTB are attributed to the absorptions of the Pr^{3+} 4*f*5*d* states. The peak at 214 nm is attributed to the transition of Pr^{3+} $^3H_4$–$^1S_0$. They all enhance as x increases, implying that the Cr^{3+} emission in the co-doped samples could be excited through the ET from Pr^{3+} $^1S_0$ to Cr^{3+}.

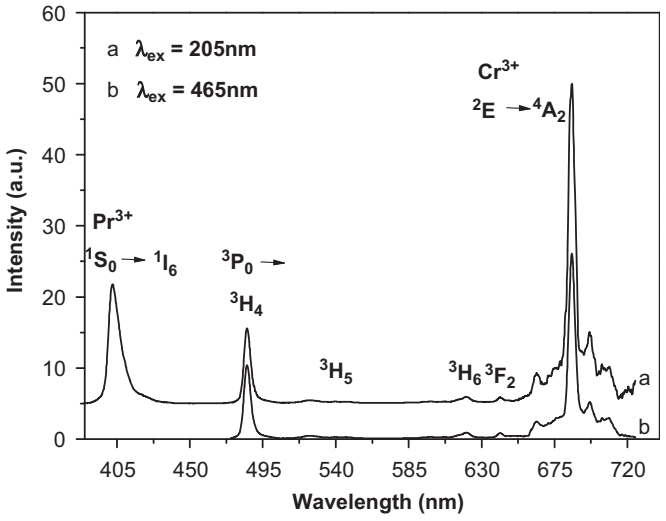

Fig. 5. Emission spectra of CAO:1% Pr, 5%Cr upon the lowest 4*f*5*d* excitation at 205 nm (a) and under $^3P_1$ excitation at 465 nm (b). Two emission spectra are scaled to the $^3P_0$–$^3H_4$ emission intensity.

The emission spectra of the typical sample of CAO:1% Pr, 5% Cr^{3+} upon excitation in the lowest 4*f*5*d* state (205 nm) and $^3P_1$ level (465 nm) of Pr^{3+} are depicted in Fig. 5. The spectra are scaled to the emissions from Pr^{3+} $^3P_0$ and the contribution of Cr^{3+} emissions by direct

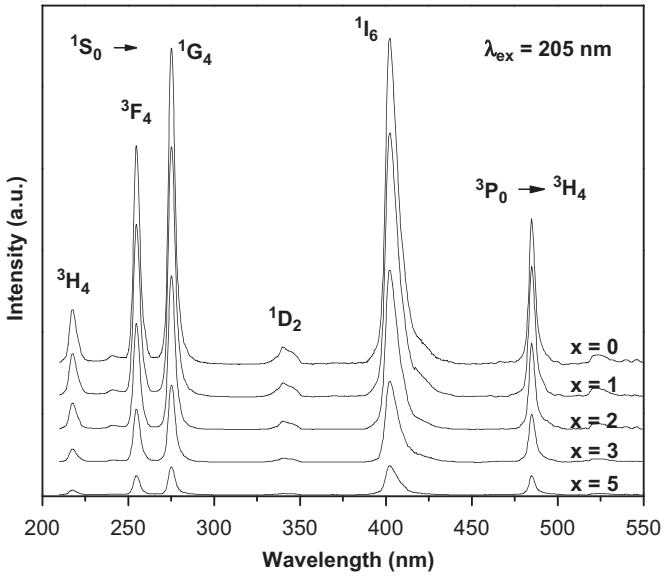

Fig. 6. Emission spectra of CAO:1% Pr, x% Cr ($x = 0$, 1, 2, 3, 5) upon 205 nm excitation. The spectra have been offset vertically for clarity.

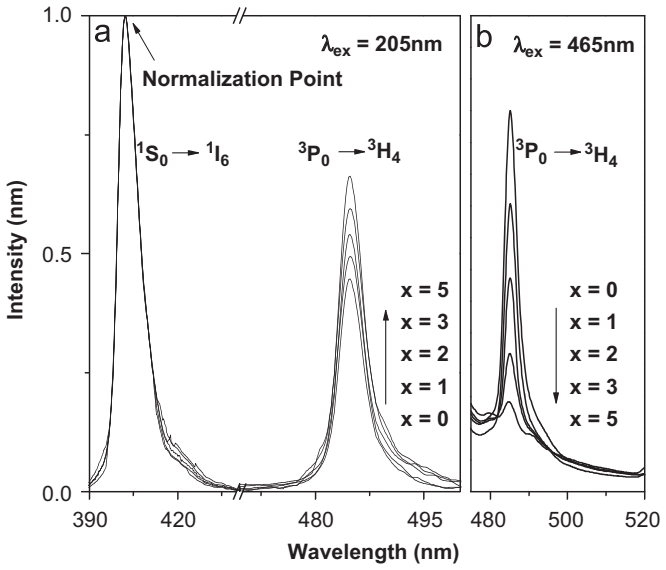

Fig. 7. (a) Normalized emission spectra of Pr^{3+} in CAO:1% Pr, x% Cr ($x = 0$, 1, 2, 3, 5), excited at 205 nm. (b) Emission spectra of Pr^{3+} $^3P_0$–$^3H_4$ transition in CAO:1% Pr, x% Cr ($x = 0$, 1, 2, 3, 5), excited at 465 nm.

excitation at 205 and 465 nm, respectively, has been subtracted by using the spectra of singly doped Cr sample. Under 465 nm excitation, the appearance of Cr^{3+} emission is in agreement with the existence of ET from Pr^{3+} ^3P_J to Cr^{3+}. The relative emission intensity of Cr^{3+} to Pr^{3+} $^3P_0$ is much higher upon 205 nm excitation compared to that upon 465 nm excitation. This observation substantiates that $^1S_0$ can transfer part of excitation energy to Cr^{3+} in addition to ^3P_J upon Pr^{3+} 4*f*5*d* excitation.

The emission spectra of Pr^{3+} in CAO:1% Pr, x% Cr ($x = 0$, 1, 2, 3, 5) upon 205 nm excitation are displayed in Fig. 6. The PCE process of Pr^{3+}, $^1S_0$–$^1I_6$ (402 nm) and $^3P_0$-$^3H_4$ (485 nm), is observed [13–15]. First, the intensities of the $^1S_0$ emissions decrease greatly as x increases, which is consistent with the presence of ET from the Pr^{3+} $^1S_0$ state to Cr^{3+}. Second, it can be carefully observed that the relative intensities of the $^3P_0$ to $^1S_0$ emissions are changed with x while those of different $^1S_0$ emissions are not. The decreasing rate of the $^3P_0$–$^3H_4$ emission is slower than those of $^1S_0$ emissions with increasing x. For example, at $x = 0$ the $^3P_0$–$^3H_4$ emission intensity is weaker than that of $^1S_0$–$^3F_4$, but when x increases to 5, the intensities of the two emission lines are about equal. Generally, upon the lowest 4*f*5*d* state excitation, the population of $^3P_0$ comes from the $^1S_0$–$^1I_6$ transition in the singly Pr^{3+}-doped sample, i.e., the $^1S_0$–$^1I_6$ emission intensity can be taken as a measure of the initial $^3P_0$ population [24]. The changes of the relative emission intensity of $^3P_0$ to $^1S_0$ with x can therefore indicate the influence of Cr^{3+} co-doping on the population of $^3P_0$. Two approaches could influence the relative intensity of $^3P_0$ to $^1S_0$ in Pr^{3+} and Cr^{3+} co-doped samples: one is CR_i, as discussed before; the other is ET_p. Actually, there is a competition between CR_i (increasing the $^3P_0$ population for higher relative intensity) and ET_p (decreasing the $^3P_0$ population for lower relative intensity).

In Fig. 7, the emission spectra of Pr^{3+} in CAO:1% Pr, x% Cr ($x = 0$, 1, 2, 3, 5) upon 205 nm excitation are normalized and compared with those under $^3P_1$ excitation by 465 nm. First, under $^3P_1$ excitation the $^3P_0$ emission decreases with increasing x, which is in accord with the occurrence of ET from the $^3P_0$ to Cr^{3+}. Second, the expected *increase* (see Section 3.2) in the relative emission intensity of $^3P_0$ to $^1S_0$ is observed clearly as x increases upon 205 nm excitation, though the ET from $^3P_0$ to Cr^{3+} can simultaneously depopulate the $^3P_0$ level resulting in the decreasing relative intensity. This observation evidences the existence and the efficiency of CR_i in the ET from Pr^{3+} $^1S_0$ to Cr^{3+}. In one word, upon VUV excitation of the lowest 4*f*5*d* state of Pr^{3+}, PCE via ET, CR_i followed by ET_p, takes place. If this ET process is efficient enough, the unpractical PCE of Pr^{3+} in $CaAl_{12}O_{19}$ will be modified into a two-red-photon luminescence of Cr^{3+} with high quantum yield.

3.4. Dynamic processes and mechanisms of ET from Pr^{3+} to Cr^{3+}

The typical decay profiles of the Pr^{3+} $^3P_0$–$^3H_4$ emission in CAO:1% Pr, x% Cr ($x = 0$, 1, 3, 5, 7) are plotted in Fig. 8. It can be seen that in the single Pr^{3+}-doped sample the fluorescence decays strictly obey the exponential rule as expected (only radiative decay). In the Pr^{3+} and Cr^{3+} co-doped sample, when the Cr^{3+} concentration is increased, the decay curve becomes more and more rapid and non-exponential, which can be explained by the introduction of extra decay pathways due to the Cr^{3+} co-doping: ET from Pr^{3+} $^3P_0$ to Cr^{3+} enhances the $^3P_0$ decay rate [25]. The non-exponential behavior can also be explained as follows. In the concentration range studied in this work the Cr^{3+} ions are randomly distributed around the Pr^{3+} lattice sites.

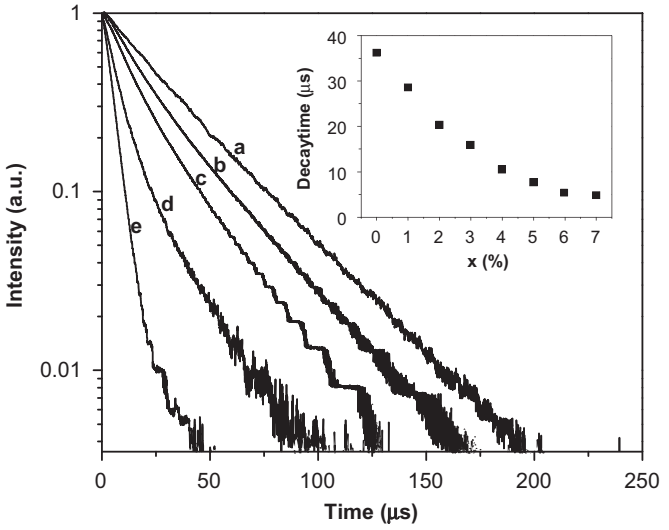

Fig. 8. Typical fluorescence decay curves of the $^3P_0$ emission in CAO:1% Pr, x% Cr, (a) $x=0$, (b) $x=1$, (c) $x=3$, (d) $x=5$, (e) $x=7$ at 465 nm excitation. Inset: Cr^{3+} concentration dependence of decay time of the $^3P_0$ emission.

The environment of every Pr^{3+} ion is different, leading to a variety of transfer rates, that is, the instantaneous average ET rate varies with time. And then, the luminescent decay curve deviates from an exponential function [26].

The difference in lifetime between samples with and without activator ions is a useful way of characterizing the ET process between sensitizer and activator ions [26]. Since the decay of Pr^{3+} ions in the presence of Cr^{3+} ions is non-exponential, the "1/e-decay time" has no physical meaning for multi-exponential decay curves. Instead, according to Inokuti–Hirayama model [27], the lifetime of a non-exponential decay curve can be defined by

$$\tau = \frac{1}{I_0}\int_0^\infty I(t)\,dt, \tag{1}$$

where I_0 is the intensity at $t=0$. Thus τ is the mean decay time, which can be obtained by integrating the decay curve over time after normalization. At $x=0$, τ_0 is about 36 μs, which is consistent with that yielded by a monoexponential fit. In the inset of Fig. 8, the τ is plotted versus Cr^{3+} concentration.

Now we will focus on the microscopic mechanism of ET from Pr^{3+} to Cr^{3+}. The microscopic mechanism of ET was first explained by Forster and Dexter [20,21]. Since there are favorable spectra overlaps of Pr^{3+} emissions and Cr^{3+} absorptions, both radiative and nonradiative transfer could be involved in the ET process.

For radiative transfer, photons emitted by donors are re-absorbed by acceptors. The pattern of donor fluorescence depends on the acceptor concentration, but the donor lifetime does not change with that [28]. As shown in Fig. 2, the spectra overlaps between various $^1S_0$ emission lines of Pr^{3+} and the absorptions of Cr^{3+} are all different. However, no obvious changes can be observed for the relative branching ratios of the $^1S_0$ emissions with or without Cr^{3+} co-doping (see Fig. 6). In addition, in our experiments the decay time of Pr^{3+} $^3P_0$ is dependent strongly on the concentration of Cr^{3+} (see Fig. 8). The results indicate that the ET in these materials is essentially a non-radiative process.

For non-radiative transfer, the transfer mechanisms, exchange (*ex*) and/or multipolar interactions, differ from one another in the dependence of the transfer rate on R_{DA}, the average distance of donor and acceptor [21,28]. According to Van Uitert formula [29]

$$C_0 = V(4\pi R_0^3/3)^{-1}, \tag{2}$$

where C_0 is the critical concentration of acceptor, at which the emission intensity or decay time of the donor is half of that without it, R_0 is the critical distance with which the ET rate is equal to the radiative decay rate from the excited donor, and V is the volume of the unit cell of CAO. By taking the experimental and analytic values of C_0 and V, about 2% for the transfer form Pr^{3+} $^3P_0$ to Cr^{3+} (see Fig. 8) and 585.83 Å [18], respectively, into the formula, R_0 is found to be about 19 Å, which is much larger than the typical critical distance for *ex* interaction (<5 Å) [21]. It indicates that the mechanism of *ex* interaction plays no role in the ET process. The multipolar character of any ET process has not only an influence on the time decay of donor luminescence but also on the concentration dependence of the macroscopic ET rate (P_{DA}). Neglecting the diffusion of excitation energy between donors, based on Dexter's ET formula of multipolar interaction the following relation can be obtained [21]:

$$P_{DA} \propto \frac{1}{R_{DA}^n} \propto x^{n/3}, \tag{3}$$

where R_{DA} also is the average D–A distance, x the ion concentration and $n=6$, 8 and 10, corresponding to dipole–dipole (d–d), dipole–quadrupole (d–q), and quadrupole–quadrupole (q–q) interactions, respectively. Thus, the dependence of the ET rate on ion concentration strongly depends on the dominant multipolar mechanism.

In addition, the macroscopic ET rate P_{DA} as a function of ion concentration can be evaluated from the lifetime measurements of the donor state since

$$P_{DA} = \frac{1}{\tau} - \frac{1}{\tau_0}, \tag{4}$$

τ_0 and τ are the decay times of the donor emission in the singly and co-doped samples, respectively [30].

Using Eqs. (1), (3) and (4) and Reisfeld's approximation the nature of interaction in this transfer process can be decided by plotting the following relation [30]:

$$\frac{I_0}{I} \propto x^{n/3} \quad \text{or} \quad \frac{\tau_0}{\tau} \propto x^{n/3}, \tag{5}$$

where I_0 and I are the luminescence intensities of Pr^{3+} with and without the presence of Cr^{3+} and $n=6$, 8 and 10 again stands for d–d, d–q, and q–q interaction mechanisms. The $\tau_0/\tau - x^{n/3}$ plots are depicted in Fig. 9 and when

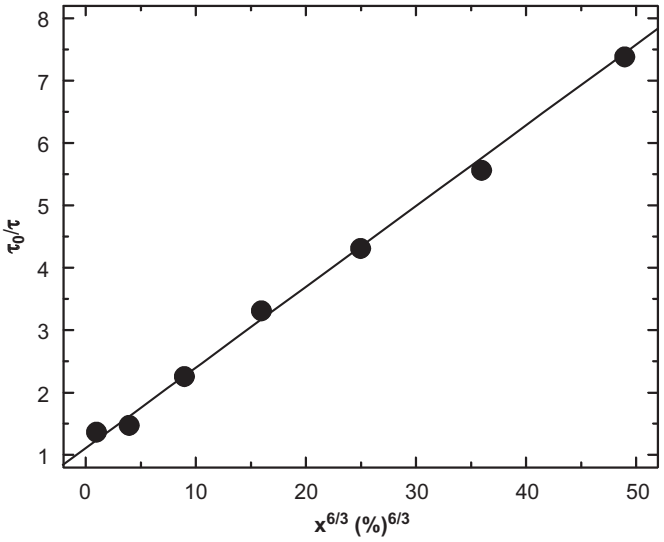

Fig. 9. Dependence of τ_0/τ of Pr^{3+} $^3P_0$ emissions on $x^{6/3}$ for CAO:1% Pr, x% Cr ($x = 1$–7). The solid line is a linear fit curve.

$n = 6$ it shows linear relation. We can then conclude that the electric d–d interaction mechanism is predominantly responsible for the ET between Pr^{3+} and Cr^{3+} ions in the co-doped CAO:Pr, Cr samples (at least in the concentration range studied in this work).

3.5. Visible QE for CAO:Pr and CAO:Pr, Cr

For single Pr^{3+} activated CAO the $^3P_0$ state is the intermediate state yielding the second photon in the cascade emission process, $^1S_0$–$^1I_6$ followed by $^3P_0$–$^3H_4$. Taking the $^1S_0$–$^1I_6$ fluorescence intensity as a measure of the initial $^3P_0$ population, the QE for $^3P_0$ yielding the second step emission, η_p, can be written as $\eta_p = R/\beta$, where R is the intensity ratio of the $^3P_0$–$^3H_4$ emission to the $^1S_0$–$^1I_6$ emission and β is the branch ratio of $^3P_0$–$^3H_4$ transition to all $^3P_0$ transitions. For CAO:1% Pr, R and β are 0.326 and 0.412, respectively, and then η_p is about 0.79 [24]. η_p decreases with increasing Pr^{3+} concentration and is significantly less than unity even at low concentration (0.5%) [24]. The total visible QE for Pr^{3+} singly doped CAO, η_{TP}, upon the lowest $4f5d$ state excitation can be written as $\eta_{TP} = \alpha(1+\eta_p\beta)$, where α (~0.49) is the branch ratio of $^1S_0$–$^1I_6$ transition to all $^1S_0$ transitions and can be obtained from the corrected luminescence spectra in Fig. 2(a). For CAO:1% Pr, η_{TP} is about 65%. If we exclude the deep violet $^1S_0$–$^1I_6$ emission, which has a poor luminous efficiency, the η_{TP} is only about 16%. Anyway, the total visible QE for CAO:1% Pr is far lower than unit.

For Pr^{3+} and Cr^{3+} co-doped CAO, the ET efficiency of CR_i, η_{CR_i} and of the sum from $^1S_0$ to Cr^{3+}, η_{Sum}, in the first step can be expressed, respectively, by

$$\eta_{CR_i} = \frac{W_{CR_i}}{W_{Sum} + \gamma_S/\alpha}, \tag{6}$$

$$\eta_{Sum} = \frac{W_{Sum}}{W_{Sum} + \gamma_S/\alpha}, \tag{7}$$

where γ_S is the rate of the $^1S_0$–$^1I_6$ transition, W_{CR_i} and W_{Sum} are the ET rates of CR_i and the sum from $^1S_0$ to Cr^{3+} in the first step, respectively, and α again is the branch ratio of $^1S_0$–$^1I_6$ transition to all $^1S_0$ transitions.

In continuous excitation upon the lowest $4f5d$ state of Pr^{3+}, the populations of the $^1S_0$ (n_S) and $^3P_0$ (n_P) states satisfy the equation $[\gamma_S + W_{CR_i}]n_S = n_P/\tau$, and then, W_{CR_i} can be expressed by

$$W_{CR_i} = \left(\frac{R\tau_0}{R_0\tau} - 1\right)\gamma_S, \tag{8}$$

where R and R_0 (~0.326) denote the intensity ratio of the $^3P_0$–$^3H_4$ emission to the $^1S_0$–$^1I_6$ emission with and without Cr^{3+} co-doping, respectively.

The absorption of Pr^{3+} at the excitation wavelength (about 200 nm, see Fig. 2) is dominant relative to that of Cr^{3+}. If we assume that the decrease of the emission intensity of Pr^{3+} $^1S_0$ is only owed to the ET from Pr^{3+} $^1S_0$ to Cr^{3+}, W_{Sum} can be estimated based on the intensity decrease of the $^1S_0$ emissions with the increase of x, as shown in Fig. 6. In continuous excitation, one has

$$W_{Sum} = \left(\frac{I_{S_0}}{I_S} - 1\right)\frac{\gamma_S}{\alpha}, \tag{9}$$

where I_S is the integral intensity of $^1S_0$–$^1I_6$ transition and I_{s_0} the integral intensity for $x = 0$.

On the other hand, from the luminescence decay curves in Fig. 8 the direct ET efficiency from Pr^{3+} $^3P_0$ to Cr^{3+}, η_{ET_p}, can be determined, which is defined as the ratio of Pr^{3+} ions that depopulate by ET to Cr^{3+} ions to the total number of Pr^{3+} ions excited. By dividing the integrated intensity of the decay curves of the CAO:1% Pr, x% Cr samples to the integrated intensity of the CAO:1% Pr curve the transfer efficiency is obtained as a function of the Cr^{3+} concentration,

$$\eta_{ET_p} = 1 - \frac{\int I_{x\%\ Cr}\,dt}{\int I_{0\%\ Cr}\,dt} \quad \text{or} \quad \eta_{ET_p} = 1 - \frac{\tau}{\tau_0}, \tag{10}$$

where I denotes intensity and x% Cr stands for the Cr^{3+} concentration.

At room temperature, the $^3P_{1,2}$ states are all the thermalized levels of $^3P_0$ and have the same luminescent dynamics [24]. Thus, they are all involved in the ET process and have the same transfer efficiency.

If we take the blue $^3P_0$–$^3H_4$ emission of Pr^{3+} into account and exclude the deep violet $^1S_0$–$^1I_6$ emission, the total visible QE for Pr^{3+} and Cr^{3+} co-doped CAO upon excitation in the lowest $4f5d$ state of Pr^{3+} can be determined using the following equation:

$$\eta_{TPC} = \eta_{Sum} + [\eta_{CR_i} + (1-\eta_{Sum})\alpha][\eta_{ET_p} + (1-\eta_{ET_p})\eta_p\beta]. \tag{11}$$

Using Eqs. (6)–(11) and the experimental data presented in Fig. 8, η_{CR_i}, η_{Sum}, η_{ET_p} and η_{TPC} can be evaluated and all

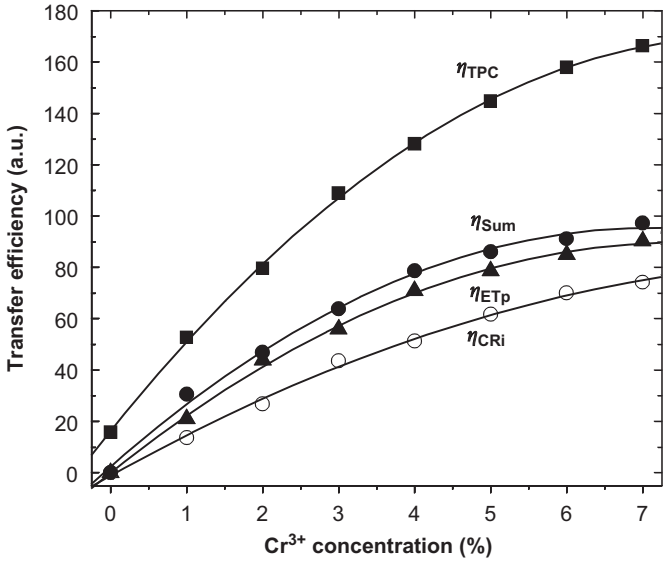

Fig. 10. Dependence of transfer efficiencies η_{CR_i} (○), η_{Sum} (●), η_{ET_p} (▲) and visible QE η_{TPC} (■) for CAO:1% Pr, x% Cr ($x = 0$–7) on Cr^{3+} concentrations. The curves are drawn as a guide to the eye.

plotted versus Cr^{3+} concentration in Fig. 10. It can be seen that the transfer efficiencies increase rapidly with increasing Cr^{3+} content. The difference between η_{Sum} and η_{CR_i}, η_{Sum}–η_{CR_i}, is smaller than η_{CR_i}, indicating that the CR_i is the main ET process from Pr^{3+} $^1S_0$ to Cr^{3+}. This is consistent with the spectral overlap between emissions of Pr^{3+} and absorptions of Cr^{3+}. According to Dexter's theory [21], the ET rate depends on the overlap integral between the emission line-shape function of the sensitizer (Pr^{3+}) and the absorption line-shape function of the activator (Cr^{3+}). The larger this spectra overlap, the more efficient the transfer process will be. As presented in Fig. 2, the spectral overlaps of the $^1S_0$–$^1I_6$ emission of Pr^{3+} with the excitation of Cr^{3+} are larger than other $^1S_0$ emissions of Pr^{3+} with Cr^{3+}.

Generally, for the ET between donor (Pr^{3+}) and acceptor (Cr^{3+}) ions, the higher acceptor dopant concentration will theoretically result in the higher trapping probability and then the higher ET efficiency. As shown in Fig. 10, the transfer efficiencies, η_{Sum} and η_{ET_p}, get closer and closer to 100% with the increase of Cr^{3+} concentration. We can assume that η_{Sum} and η_{ET_p} could approximately be equal to 1 if x is high enough, i.e., the $^1S_0$ and $^3P_0$ states could transfer all of their energies to Cr^{3+}. And then, following Eq. (11), the maximal visible QE $\eta_{TPC} \approx 1 + \eta_{CR_i}$. According to Fig. 10, when $x > 5$, $\eta_{CR_i} > 70\%\ \eta_{Sum}$, that is, more than 70% energy was transferred to Cr^{3+} through CR_i in the transfers from $^1S_0$ to Cr^{3+} (CR_i, CR_f, CR_g and ETs). Thus the maximal η_{TPC} could reach more than 170%. The visible QE is much higher than unity and may seem exciting. But unfortunately, it cannot be achieved. Firstly, in a practical VUV phosphor based on the Pr^{3+}–Cr^{3+} pair, the Pr^{3+} ion and not the Cr^{3+} should absorb the VUV emission from the Xe discharge (located between 149 and 173 nm) of the eventual application. As shown in Fig. 2, it becomes evident that Cr^{3+} ions will be involved in the absorption just as well as Pr^{3+} ions in the VUV region. Direct Cr^{3+} excitation will result in a normal one-photon emission process, which lowers the total QE of the two-photon-luminescence. Secondly, η_{TPC} is dependent on the dopant concentrations of Pr^{3+} and Cr^{3+} and their concentration ratios. The dopant concentration of Pr^{3+} must be high enough that can ensure that phosphor has a strong absorption or a big absorption cross-section in the VUV region. But higher concentration wants higher trapping probability and too high concentration will bring out concentration quenching. The critical quenching concentration of Pr^{3+} due to the cross relaxation of $^3P_0$ is more than 5% in CAO (this work). For the dopant concentration of Cr^{3+}, too high concentration will result in the direct excitation of Cr^{3+} instead of Pr^{3+} and also the occurrence of concentration quenching. Thus, the realization of the maximum η_{TPC} is dependent on the optimal excitation wavelength and the optimum concentrations of Pr^{3+} and Cr^{3+} and their concentration ratios. In our present work, the series of CAO:1% Pr, x% Cr ($x = 1$–10) samples were chosen and the excitation of the lowest $4f5d$ state of Pr^{3+} at about 200 nm was selected, where the absorption of Cr^{3+} is very weak and is ignored in this work.

As shown in Fig. 11, the dependence of Cr^{3+} emission intensities on Cr^{3+} concentration in CAO:1% Pr, x% Cr ($x = 1$–10) upon Pr^{3+} excitation at 205 nm and under direct Cr^{3+} excitation at 550 nm are presented. The emission intensities at $x = 1$ in the two samples have been normalized. Under different excitations, both emission intensities approach maximum at Cr^{3+} content about 5%, then they decrease. From curve (a), the critical quenching concentration of Cr^{3+} can be determined to be about 5%

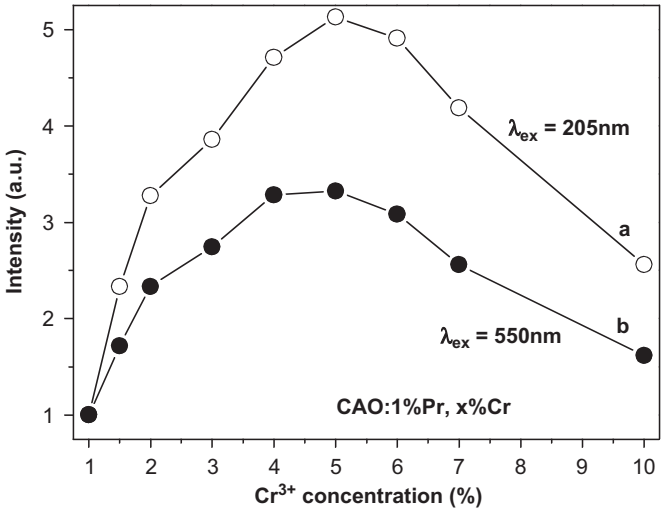

Fig. 11. Dependence of emission intensity of Cr^{3+} on the Cr^{3+} concentration in CAO:1% Pr, x% Cr ($x = 1$–10) under 205 nm (a) and under 550 nm excitations (b). The emission intensities at $x = 1$ in the two samples have been normalized.

in CAO. With the increasing Cr^{3+} content, for the climbing phase the emission intensities upon Pr^{3+} excitation increase faster than that under Cr^{3+} excitation, which shows that the ET from Pr^{3+} to Cr^{3+} increases the luminescence output of Cr^{3+}. However, upon Pr^{3+} excitation at Cr^{3+} concentration higher than 5%, although the ET efficiency will continue to increase, as discussed above, the actual luminescence output of the Cr^{3+} ions will decrease in the same way due to the concentration quenching of Cr^{3+}. When the Pr^{3+} concentration is fixed at 1%, the optimum concentrations for Cr^{3+} is about 5%. As shown in Fig. 10, for $x = 5$, $\eta_{CR_i} = 61\%$, $\eta_{Sum} = 86\%$, $\eta_{ET_p} = 78\%$ and $\eta_{TPC} = 143\%$ are obtained. But considering the Cr^{3+} ions will compete with the Pr^{3+} ions under the radiation from the Xe discharge, we believe that the actual visible QE as a practical VUV phosphor will be depressed greatly.

4. Conclusions

The Cr^{3+} ion was chosen as a co-dopant to modify the unpractical PCE properties of Pr^{3+} in $CaAl_{12}O_{19}$ phosphors. There exists a favorable spectra overlap between the emission spectra of the Pr^{3+} and the excitation spectra of the Cr^{3+} in CAO, which promotes a two-step ET from Pr^{3+} to Cr^{3+}, converting the photon from Pr^{3+} $^1S_0$ in the unpractical UV or near-UV region into the red Cr^{3+} emission through cross-relaxations, and subsequently, photon from Pr^{3+} $^3P_0$ also into the red Cr^{3+} emission through direct ET. The Dexter model was applied to the analysis of the concentration dependence of the ET rate from Pr^{3+} $^3P_0$ to Cr^{3+}, which indicated that the d–d interaction mechanism is mainly responsible for the transfer. Upon excitation into the lowest $4f5d$ state of Pr^{3+}, the two-step ET between Pr^{3+} and Cr^{3+} is efficient and a visible QE higher than 100% can be achieved, but considering the Cr^{3+} ions will compete with the Pr^{3+} ions under the radiation from the Xe discharge, we believe that the actual visible QE as a practical VUV phosphor will be depressed greatly.

Acknowledgments

This work is financially supported by the MOST of China (2006CB601104, 2006AA03A138), the National Natural Science Foundation of China (10574128, 10504031) and by the Cotrell College Science Awards from Research Corporation.

References

[1] G. Blasse, B.C. Grabmeier, Luminescent Materials, Springer, Berlin, 1994.
[2] Recent developments in photon cascade emission phosphors have been reviewed, in: A.M. Srivastava (Ed.), Encyclopedia of Physical Science and technology, third ed., vol. 11, Academic Press, New York, 2002, p. 855.;
A.M. Srivastava, in: H.S. Nalwa, L.S. Rowher (Eds.), Handbook of Luminescence, Display Materials, and Devices, vol. 3, American Scientific Publishers, 2003, p. 79.
[3] S. Kuck, I. Sokolska, M. Henke, M. Doring, T. Scheffler, J. Lumin. 102–103 (2003) 176.
[4] A.P. Vink, P. Dorenbos, C.W.E. van Eijk, J. Solid State Chem. 171 (2003) 308.
[5] P.A. Rodnyi, S.B. Mikhrin, P. Dorenbos, E. van der Kolk, C.W.E. van Eijk, A.P. Vink, A.G. Avanesov, Opt. Commun. 204 (2002) 237.
[6] M. Zachau, F. Zwaschka, F. Kummer, Proc.-Electrochem. Soc. 97–29 (1998) 314.
[7] E. van der Kolk, P. Dorenbos, C.W.E. van Eijk, A.P. Vink, M. Weil, J.P. Chaminade, J. Appl. Phys. 95 (2004) 7867.
[8] P. Vergeer, V. Babin, A. Meijerink, J. Lumin. 114 (2005) 267.
[9] S. Kuck, I. Sokolska, J. Phys.: Condens. Matter 18 (2006) 5447.
[10] Y. Chen, C. Shi, Z. Qi, Y. Fu, Appl. Phys. Lett. 88 (2006) 061906.
[11] Z. Nie, J. Zhang, X. Zhang, X. Ren, W. Di, G. Zhang, D. Zhang, X. Wang, J. Phys.: Condens. Matter 19 (2007) 076204.
[12] E. van der Kolk, P. Dorenbos, C.W.E. van Eijk, A.P. Vink, C. Fouassier, F. Guillen., J. Lumin. 97 (2002) 212.
[13] A.M. Srivastava, W.W. Beers, J. Lumin. 71 (1997) 285.
[14] A.M. Srivastava, D.A. Doughty, W.W. Beers, J. Electrochem. Soc. 143 (1996) 4113.
[15] A.M. Srivastava, D.A. Doughty, W.W. Beers, J. Electrochem. Soc. 144 (1997) 190.
[16] S.R. Jansen, H.T. Hintzen, R. Metselaar, Fourth Euro-Ceramics—Basic Science—Developments in Processing of Advanced Ceramics—Part II, Gruppo Editoriale Faenza Editrice S.p.A., Italy, 1995, p. 353.
[17] X. Wang, S. Huang, L. Lu, W.M. Yen, A.M. Srivastava, A.A. Setlur, Opt. Commun. 195 (2001) 405.
[18] A. Utsunomiya, K. Tanaka, H. Morikawa, F. Marumo, J. Solid State Chem. 75 (1988) 197.
[19] R.D. Shannon, Acta Crystallogr. Sect. A: Cryst. Phys. Diffr. Theor. Gen. Crystallogr 32 (1976) 751.
[20] Th. Forster, Ann. Phys. 2 (1948) 55.
[21] D.L. Dexter, J. Chem. Phys. 21 (1953) 836.
[22] H.H. Tippins, Phys. Rev. B 1 (1970) 126.
[23] B. Henderson, G.F. Imbush, Optical Spectroscopy of Inorganic Solids, Oxford Science Publications, Oxford, 1989.
[24] S. Huang, X. Wang, B. Chen, D. Jia, W.M. Yen, J. Lumin. 102–103 (2003) 344.
[25] G. Blasse, B.C. Grabmarier, Luminescent Materials, Springer, Berlin, Germany, 1994 (p. 96).
[26] D. Huber, in: W.M. Yen, P.M. Selzer (Eds.), Laser Spectroscopy of Solids, Springer, Berlin, 1981, p. 83.
[27] M. Inokuti, F. Hirayama, J. Chem. Phys. 43 (1965) 1978.
[28] L.G. Van Uiter, L.F. Johnson, J. Chem. Phys. 44 (1966) 3514.
[29] L.G. Van Uitert, J. Lumin. 4 (1971) 1.
[30] R. Reisfeld, N. Lieblich-sofer, J. Solid State Chem. 28 (1979) 391.